Cellulose (2018) 25:179–194
https://doi.org/10.1007/s10570-017-1602-5

ORIGINAL PAPER

Effect of lignin on the morphology and rheological properties of nanofibrillated cellulose produced from γ-valerolactone/water fractionation process

Huy Quang Lê · Katarina Dimic-Misic · Leena-Sisko Johansson · Thaddeus Maloney · Herbert Sixta

Received: 24 August 2017 / Accepted: 1 December 2017 / Published online: 12 December 2017

Abstract The influence of lignin content on nanocellulosic fibril morphology, charge, colloidal stability and immobilization has been systematically investigated employing a series of nanofibrillated cellulose (NFC) with varying residual lignin content and compared to those of NFC made from fully bleached pulp. The lignin-containing pulps were obtained from the fractionation of *Eucalyptus globulus* wood chips in gamma-valerolactone (GVL)/water under the same conditions, they differ by the intensity of washing for lignin removal. The reference pulp originated from another cook of eucalyptus wood chips, and was fully bleached with a short Elemental-Chlorine-Free (ECF) sequence. All the pulps have a comparable hemicellulose-to-cellulose ratio and CED viscosity. NFC suspensions of 1 wt% concentration were mechanically produced from fluidization. The results indicated that the fibrils morphology, thickness and corresponding flocculation within NFC suspensions was highly influenced by the presence of lignin unevenly distributed on the fibril surface and within the suspension as particles. The presence of lignin in NFC suspension had a large impact on the rheology and dewatering of the NFC. Samples with high lignin content had distinguishable viscoelastic properties due to the greater flocculation of thicker fibrils and lower gel-like characteristics, with better dewatering properties.

Keywords Nanocellulose · Lignin · Dissolving pulp · Rheology · Gamma-valerolactone

Electronic supplementary material The online version of this article (https://doi.org/10.1007/s10570-017-1602-5) contains supplementary material, which is available to authorized users.

H. Q. Lê · K. Dimic-Misic · L.-S. Johansson · T. Maloney
School of Chemical Engineering, Department of Bioproducts and Biosystems, Aalto University, Vuorimiehentie 1, 02130 Espoo, Finland
e-mail: huy.le@aalto.fi

K. Dimic-Misic
e-mail: katarina.dimic.misic@aalto.fi

L.-S. Johansson
e-mail: leena-sisko.johansson@aalto.fi

T. Maloney
e-mail: thaddeus.maloney@aalto.fi

H. Sixta (✉)
School of Chemical Engineering, Department of Bioproducts and Biosystems, Aalto University, Vuorimiehentie 1, P.O. Box 16300, 02130 Espoo, Finland
e-mail: herbert.sixta@aalto.fi

Introduction

With the global production of billions of tons per annum (Lieth 1975), lignocellulosic biomass is the most promising sustainable resources to replace the

depleting fossil feedstock (Huber et al. 2006). Wood, the most important lignocellulosic biomass, is a natural composite composed mainly of cellulose, hemicelluloses and lignin (Sjöström 1993), with the former comprising about 40–50% of the dry mass, making it the most abundant renewable polymer on Earth. Regardless of the source, cellulose is a linear, semi-crystalline homo-polysaccharide of β-D-glucopyranose units linked together by β-1-4 glycosidic bonds, forming the repeating unit of cellobiose (Sjöström 1993). Bioproducts from cellulose are naturally the most significant among the spectrum of biomass-derived products. Currently, the main cellulosic commodities are paper-grade pulp and dissolving pulp, with a global annual production of about 170 million tons and 6.4 million tons (2013), respectively (Conley 2014; Young 2014). Recently, novel applications employing nano-sized cellulosic material has attracted increasing attention due to their distinctive characteristics such as biodegradability, modifiability, reactivity, high aspect ratio, outstanding mechanical properties, good barrier properties and unique optical properties (Fukuzumi et al. 2009; Moon et al. 2011). Nanocelluloses are generally divided into three subcategories of bacterial cellulose, cellulose nanocrystal, and nanofibrillated cellulose. In this study, we specifically emphasize on NFC, the smallest unit of plant fibers, which is a bundle of entangled cellulose chains consisting of alternating amorphous and crystalline domains, with the typical width of 5–20 nm and the length of several hundred nanometers (Klemm et al. 2005; Saito et al. 2006; Sakurada et al. 1962).

The production of nanofibrillated cellulose (NFC) from lignocellulosic biomass is lengthy and energy intensive. Typically, wood is chemically fractionated into a cellulose-rich pulp fraction, which is subsequently chemically bleached to remove residual lignin, then mechanically disintegrated at low consistency into NFC. Extensive research effort has been made on reducing the energy consumption the NFC production. The most popular approach is the incorporation of a pretreatment step before mechanical disintegration, with enzymatic treatment (Janardhnan and Sain 2007; Pääkkö et al. 2007) or TEMPO-oxidation (Saito and Isogai 2004) being the most efficient methods. However, alternative pulping process can also positively affect the overall economy of the NFC production. Currently, NFC predominantly originates from bleached kraft pulp with typically high (more than 20%) hemicellulose content. However, dissolving pulp could be the preferred substrate to produce NFC for application requiring higher purity of cellulose. We suggested a novel sulfur-free organosolv fractionation process employing aqueous γ-valerolactone (GVL) solution (Lê et al. 2016) that enables the one-step production of dissolving pulp which can be readily converted to NFC. This process excels pre-hydrolysis kraft or sulfite pulping in term of pulp yield, simplicity and environmentally friendliness (Lê et al. 2016), thus potentially reduces the production cost of low-hemicellulose-content NFC. Lastly, the residual lignin fraction of the pulp has a significant effect on the process economy. Even though NFCs are generally manufactured from lignin-free fully-bleached pulp, utilizing unbleached pulp offers several benefit such as higher yield, lower environmental impact due to the elimination of the bleaching sequence, which typically contains chlorine. Moreover, lignin-containing NFC might exhibit interesting characteristics related to the hydrophobicity and glue-like properties of lignin (Ferrer et al. 2012; Nelson et al. 2016). NFC originated from unbleached dissolving pulp has not gained enough research attention. Therefore, in this work, we extensively characterized this type of NFC suspension as a basis for revealing its possible applications.

As mentioned earlier, NFC is typically produced in the form of low consistency (less than 10 wt%) aqueous suspensions, of which their rheological properties significantly affect their processability. For the rheological characterization of NFC suspensions it is necessary to employ different protocols in order to compare the results qualitatively rather than quantitatively (Martoia et al. 2015; Mohtaschemi et al. 2014). A major challenge in rheologically investigating the NFC suspensions is to avoid the wall-slip effect arising from the depletion layer of dispersed particles from the contact region with the measurement geometry. That phenomenon leaves a liquid layer at the geometry wall having a lower viscosity than the bulk viscosity (Nazari et al. 2016; Nechyporchuk et al. 2014; Puisto et al. 2012). The use of serrated surfaces in plate-plate rheometry and the adoption of a vane spindle in the bob-in-cup geometry were reported to decrease the wall-slip effect (Dimic-Misic et al. 2014b; Mohtaschemi et al. 2014; Nechyporchuk et al. 2014). Additionally, the application of shear on fibrillar hydrogels in the bob-in-cup geometry, without

the adoption of the vane, was found to induce the changes in the flocculation structure and shear-banding effect (Karppinen et al. 2012; Martoia et al. 2015), resulting in the phase separation tendency and influencing the thixotropic properties (Buscall 2010; Nechyporchuk et al. 2014). The rheological properties vary upon the morphology and surface charge of the nanofibrils, the temperature and consistency of the suspension, which in turn have an effect on the processibility and interaction between the fibrils (Dimic-Misic et al. 2013b; Fall et al. 2009; Lasseuguette et al. 2008).

Industrial applications of NFC suspensions require medium-to-high solids consistency to ensure the process economy. Dewatering is thus a challenge due to the strong water-holding capacity of the nanofibrillar gel (Rudraraju and Wyandt 2005; Usov et al. 2015). The phase separation process of aqueous NFC suspension depends on the flocculation structure and the electrostatic properties of the fibrils which bind water and form the regions of interstitially held water, affecting the gelation within the suspension (Dimic-Misic et al. 2014a; Nazari et al. 2016). Mixing time and shear rate have a strong influence on the rheological response of the system, as they are in many cases strongly interrelated (Dalpke and Kerekes 2005; Tanaka et al. 2014). When shearing beyond the yield point of the viscoelastic structure, phase separation can be achieved under external pressure or vacuum by breaking the gel or flocculation within the fibrillar network, thus inducing the dewatering phenomenon (Bonn et al. 2002; Chaari et al. 2003; Dentel et al. 2000; Dimic-Misic et al. 2013b). Therefore, it is favorable to tailor the NFC suspensions to a lower surface charge and lower water binding properties, which reduces the swelling and improves the flocculation, which in turn induces the phase separation between fibrillar matrix and water and reduces the problems related to pure dewatering (Pääkkönen et al. 2016).

In this study, unbleached dissolving pulps were obtained from GVL/water fractionation of *Eucalyptus globulus* wood chips with varying washing intensity in order to tailor the lignin content while keeping the hemicellulose/cellulose ratio and the cellulose degree of polymerization constant. Lignin-containing NFC suspensions were produced from the unbleached pulps by pure mechanical treatment, which were then subjected to an extensive analysis array in order to reveal their morphological, topological, rheological and water retention properties.

Experimental

Materials

Eucalyptus globulus wood chips were delivered by ENCE, Spain. The chips were screened according to the SCAN-CM 40:01 standard and stored at − 20 °C until further usage. The identified chemical composition of the wood was 44.1% glucose, 15.2% xylose, 3.1% other sugars, 27.7% lignin and 1.3% extractive. The GVL was supplied by Sigma Aldrich with ≥ 98 wt% purity. Pure water, with a resistivity of 18.2 MΩ cm, was produced on site using a Millipore Synergy® UV purification system.

Pulps production and characterization

Eucalyptus globulus wood chips were fractionated in an aqueous solution of GVL at elevated temperature without the presence of any catalyst or additives. The fractionation experiments were conducted in 2.5 L autoclaves heated in an air-bath digester (Haato Oy 16140-538). The lignin-containing pulps originated from the same cook, and their residual lignin content was adjusted by controlling the pulp washing intensity. A reference pulp with no residual lignin was obtained from a separate cook followed by an ECF bleaching. The pulp production scheme is illustrated in Fig. 1. Details of the fractionation and bleaching processes are presented in Appendix A.

The carbohydrate and lignin content in the pulps was analyzed in accordance to the 2-step hydrolysis method described in the NREL/TP-510-42618 standard. The pulp was firstly hydrolyzed in 72% H_2SO_4, with an acid-to-material ratio of 10 mL/g, at 30 ± 3 °C, for 60 ± 5 min. The hydrolyzed suspension was subjected to the second hydrolysis in 4% H_2SO_4, with an acid-to-material ratio of 300 mL/g, at 121 ± 1 °C, for 60 min. The monosaccharides were analyzed by High Performance Anion Exchange Chromatography (HPAEC-PAD) in a Dionex ICS-3000 system, equipped with CarboPac PA20 column. From the amount of neutral monosaccharides, the cellulose and hemicelluloses content in wood and pulp samples was estimated with the formula introduced by

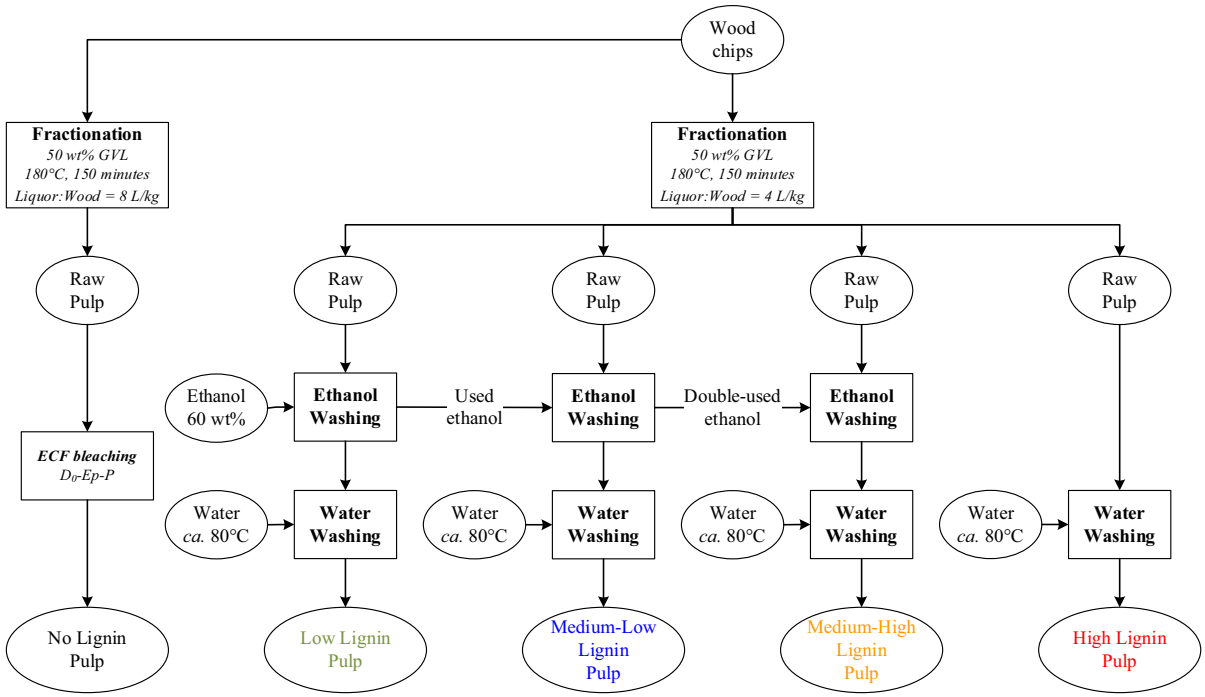

Fig. 1 Production of pulps with different amount of residual lignin by GVL/water fractionation. Washing of bleached pulp is not shown for simplification purpose. (Color figure online)

(Janson 1970). The amount of acid insoluble (Klason) lignin was gravimetrically determined while the amount of acid soluble lignin (ASL) was determined by measuring the absorbance at the wavelength of 205 nm by the Shimadzu UV-2550 spectrophotometer. An extinction coefficient of 148 L/(g.cm) was used for quantification of ASL (Lê et al. 2016). The pulps were analyzed for their intrinsic viscosity in cupriethylenediamine (CED) and their kappa number in accordance to the SCAN-CM 15:88 and SCAN-C 1:00 standards, respectively. All the analyses were performed in duplicate for each pulp sample.

NFC suspensions production and characterization

NFCs suspensions with different amount of residual lignin were produced from the 5 pulps produced as described in "Pulps production and characterization" section. The pulps were diluted to 1 wt% consistency and disintegrated according to the ISO 5236-1 standard. NFC was obtained from a 12-pass fluidization of the 1 wt% pulp suspension by a Microfluidics M-110P fluidizer through a chamber nozzle pair with diameters of 200 and 100 μm at a constant pressure of 1000 bar.

Nano-scale topography of the NFC was investigated by Atomic Force Microscopy (AFM) using a MultiMode 8 atomic force microscope with a Bruker NanoScope V controller. NFC gel sample was diluted with water by the dilution factor of 100 then dry-cast onto a Mica support for AFM imaging. The images were obtained by scanning the sample surface in tapping mode with MicroMasch HQ:NSC15/Al BS p robes at resonance frequencies of 265–410 kHz. At least three locations on each sample were scanned at image sizes of 5×5 μm^2, and 2×2 μm^2. AFM images were processed and analyzed with Bruker NanoScope Analysis 1.5 software. The images were flattened, the fibril and lignin particle dimensions were analyzed from the height images with the section tool. At least ten different sections from separate NFC fibrils of each image were analyzed.

Nano-scale morphology of the NFC was examined by Scanning Electron Spectroscopy (SEM) using a Zeiss Sigma VP scanning electron microscope. Freeze-dried NFC aerogel samples installed onto double-sided carbon tapes were coated with a 4.1 nm-thick gold–palladium layer by Leica EM ACE 600 High Vacuum Sputter Coater. The operating

voltage was either 1.5 or 2 kV, the working distance was 3.4–4.9 mm and the magnification was about 30 000 times. Optical microscope image between crossed polarizers was obtained with a polarizing microscope Leica DM4500 P equipped with a Leica DFC420 camera.

Water retention value (WRV) of the NFC was determined in accordance to the standard SCAN-C 102XE with a slight modification that a polyamine monofilament open mesh fabric SEFAR NITEX® 03–1/1 with a pore size of 1 μm was placed on top of a 125 μm metal screen. The experiment was performed in triplicate for each sample.

The static gravimetric dewatering of suspensions was measured according to the Åbo Akademi Gravimetric Water Retention method (ÅA-GWR) (Sandas et al. 1989). 10 ml of NFC suspension was inserted into the cylindrical vessel above a 0.5 μm polycarbonate membrane (Whatman® Nucleopore Track-Etch) and absorbent blotter papers. The cylinder was closed and the sample was held under a vacuum of 50 kPa for 105 s, during which time dewatering through the membrane occurred. The blotter paper sheet/stack was weighed before the start of the dewatering measurement and after when the pressure was released. The weight difference was multiplied by 15 091 m^{-2}, which is the inverse of the cylinder cross-sectional area. The experiment was performed 5 times for each sample.

Surface charge of the nanofibrils was assessed via their zeta potentials measured in a dip cell probe with a Malvern Zetasizer Nano-ZS90 Instrument. The experiment was repeated 10 times for each samples.

NFC films production and characterization

The films were prepared by pressurized filtration method introduced by (Österberg et al. 2013). A film was form by the filtration of a 150 mL portion of 0.84% NFC suspension under 2.0 bar pressure through a polyamine monofilament open mesh fabric SEFAR NITEX® 03-10/2 with 10 μm pore size, for about 15 min. The films were hot-pressed in a Carver Laboratory press at about 100 °C and 22.0 bar for 2 h. Before any characterization, the films were stored at 23 °C and 50% relative humidity for at least 72 h according to the ISO 291:2005 standard.

Mechanical properties of lignin-containing NFC films were measured by a MTS 400/M vertical tensile tester equipped with a 20 N load cell. The instrument were controlled by the TestWorks 4.02 program. Specimen strips with dimensions of (60 × 15) mm^2 were clipped from the NFC films with a lab paper cutter. The thickness of the strips was separately measured with a L&W micrometer SE 250. The gauge length was 40 mm and the testing velocity was 0.5 mm/min. The results are presented as an average value obtained from five parallel specimens.

The water contact angle of NFC films was determined with a KSV CAM200 optical contact angle goniometer. The tests were performed at room temperature, the contact angle after 2 s since the contact time was recorded and the results are presented as an average value of at least four experiments.

Surface composition and surface lignin content of the NFC films were evaluated with X-ray photoelectron spectroscopy (XPS), using a Kratos AXIS Ultra electron spectrometer, with monochromatic Al Kα irradiation at 100 W and under neutralization. Prior to the analysis, the samples were extracted with acetone for 6 h by the Soxhlet apparatus in order to differentiate the lignin from surface passivation species and the extractive remnants (Johansson et al. 2011; Koljonen et al. 2003). Both the unextracted and extracted specimens were analyzed. For the experiment, samples were pre-evacuated for at least 12 h, after which wide area survey spectra (for elemental analysis) as well as high resolution regions of C1 and O1 s were recorded from several locations, and an in situ reference of pure cellulose was recorded for each sample batch (Johansson and Campbell 2004). With the parameters used, XPS analysis was recorded on an area of 1 mm^2 and the analysis depth is less than 10 nm. Carbon high resolution data was fitted using CasaXPS and a four component Gaussian fit tailored for celluloses (Johansson and Campbell 2004). The surface coverage of lignin was calculated with the pure cellulose sample as the reference material, as described by (Koljonen et al. 2003).

NFC rheological analyses

Rheological properties of lignin-containing NFC suspensions were analyzed at 23 °C with an Anton Paar MCR 300 shear rheometer.

Oscillatory measurements, which revealed the suspension behaviors within the Linear Viscoelastic Region (LVR), were performed using the serrated

plate-plate geometry, where the upper plate has a diameter of 25 mm and the gap between the plates was set at 1 mm (Dimic-Misic et al. 2013a, b). In order to avoid strain accumulation within the thixotropic nanocellulose gel-like matrix upon loading the sample to the rheometer, prehearing protocol was used, as reported earlier for similar materials (Dimic-Misic et al. 2013a). The pre-shear protocol was angular frequency (ω) of 10 rad s^{-1} and strain (γ) of 0.01% for 5 min, followed by a rest time of 15 min (Moan et al. 2003). The LVR of the samples was determined via the amplitude sweep oscillatory tests. The angular frequency sweep tests were then performed with decreasing frequency of $\omega = 100 - 0.01$ rad s^{-1}, with a logarithmic spread of data points. In order to prevent the water evaporation during the rheological measurements, a layer of silicone oil was spread over the sample surface which was in contact with the air (Moan et al. 2003).

The dynamic viscosity (η) was determined by steady shear-flow measurements, using the bob-in-cup geometry. The "bob" was a four-bladed vane spindle with a diameter of 10 mm and a length of 8.8 mm, while the metal cup had a diameter of 17 mm. The pre-shear protocol was $\dot{\gamma} = 100$ s^{-1} for 5 min, followed by a rest time of 10 min. Flow curves of NFC suspensions were constructed with decreasing shear rate of $\dot{\gamma} = 1000 - 0.01$ s^{-1}, with a logarithmic spread of data points.

Shear thinning behavior

In order to distinguish the NFC suspensions in terms of their colloidal interactions, packing effects and friction between nanofibrils during the flow, the log–log plot flow curves of both complex viscosity (η*) and dynamic viscosity (η) were fitted to a power law according to the Oswald–de Waele empirical model (Dimic-Misic et al. 2013a, b; Lasseuguette et al. 2008; Pääkkönen et al. 2016), as shown in Eq. (1).

$$\eta = k\dot{\gamma}^{-n} \tag{1}$$

where k and n are the flow index and the power-law exponent, respectively. $n = 0$ indicates a Newtonian fluid and $n > 0$ indicates pseudo-plastic (shear thinning) behavior (Dimic-Misic et al. 2013b).

Yield stress

Due to the thixotropic behavior of gel-like NFC suspensions which are prone to wall-slip at high shear rates, yield stress was obtained from both oscillatory and steady shear rheometry. Model fitting of the log–log plot of the flow curve from shear flow measurements was employed for determining the dynamic yield stress (τ_d^0), which was the dynamic stress (τ_d) that plateaued at low shear rate (Yang et al. 1986). The Herschel–Bulkley equation describes the dynamic yield stress τ_d^0 in NFC suspension (Martoia et al. 2015; Mohtaschemi et al. 2014; Nechyporchuk et al. 2014; Puisto et al. 2012).

$$\tau = \tau_d^0 + k\dot{\gamma}^n \tag{2}$$

where τ_d, k and n are the measured stress, the consistency and the flow index, respectively. For $n < 1$, the material exhibits shear thinning, and for $n = 1$, Newtonian behavior.

However, fitting the dynamic stress flow curve data to a yield stress model can lead to a misconception of the dynamic yield stress determination (τ_d^0), especially with the rheologically complex thixotropic gel-like suspensions, in which the maintenance of flow is much less energy demanding than the initiation of flow due to the normally very long time constant for the re-establishment of the gel structure (Fall et al. 2009; Karppinen et al. 2012; Lasseuguette et al. 2008). Therefore, in the case of NFC gels, it is preferable to compare the yield stress obtained from oscillatory experiments within the LVR regions, to the dynamic yield stress (τ_d^0) (Nazari et al. 2016). The static stress component (τ_s) in oscillatory measurements is given in Eq. 3.

$$\tau_s^0 = G'\gamma \tag{3}$$

As strain (γ) constantly increased at constant frequency (ω) in the oscillatory amplitude sweep measurements, the maximum in the elastic stress (τ_s) corresponding to the static elastic yield stress (τ_s^0) was determined as the first point of deviation from the linear elastic deformation occurring at a corresponding critical strain value (γ_c) (Pääkkönen et al. 2016).

Due to the rheological complexity of thixotropic and shear banding NFC suspensions, the apparent dynamic yield stress (τ_d^0) was determined by the Herschel–Bulkley model in the low shear rate domain

of 0.01–0.1 s^{-1} (Karppinen et al. 2012; Lasseuguette et al. 2008; Pääkkönen et al. 2016). The flow coefficient k and power law coefficient n are obtained by linearization of the shear stress (τ_d–τ^0_{d0}) against the shear rate log–log curves (Pääkkönen et al. 2016), where τ^0_{d0} is the minimum value of dynamic stress.

Recovery measurements

Structural recovery of NFC suspensions was analyzed with the oscillatory and rotational Three Interval Thixotropic Tests (3ITT). Oscillatory 3ITT tests were performed using the plate-plate geometry. The evolution of the elastic moduli (G′) was traced by applying a high shear interval of 1000 s^{-1} between two oscillatory intervals within the LVR at constant strain of 0.1% and at constant angular frequency of 10 rad s^{-1}. Recovery of the elastic moduli (G′) was traced with reduced elastic moduli (G'/G'_0) in the third interval, as a rate of suspension elasticity recovery after the structural breaking–up during shearing. Rotational 3ITT test were performed using the bob-in-cup geometry. In this test, the evolution of transient viscosity (η^+) after the high shear rate period was found by applying a step-wise shear rate with three defined intervals of applied shear, namely a low shear interval-high shear interval-low shear interval procedure. During the first and third intervals, the sample was subjected to a low shear rate of 0.1 s^{-1}, and in the second interval, to a high shear rate of 1000 s^{-1}. Recovery of structure after high shear (during the second interval) was calculated after 300 s from the start-up of the third interval (low shear), as the value of the reduced transient viscosity (η^+/η^+_0), where η^+_0 is the dynamic viscosity value during the first interval.

Rheological data processing and reproducibility

Rheological measurements were performed five times for each sample, including the pre-shearing, and for the calculation of rheological parameters, the average values of five measurements were used with deviations. However, due to the rheological complexity of the NFC systems containing thixotropic gel-like

Table 1 Properties of the pulps with different amount of residual lignin and their corresponding NFC suspensions and films

Properties	No–L	L–L	ML–L	MH–L	H–L
Pulps properties					
Kappa number	0.6	7.3	16.2	27.1	59.4
Lignin content (%odp)	0.2	1.7	3.1	4.9	10.5
Adsorbed lignin (%odp)	0.0	0.0	1.4	3.2	8.8
Cellulose (%odp)	93.0	91.7	90.4	88.7	83.6
Hemicellulose (%odp)	6.8	6.6	6.5	6.4	5.9
Hemicellulose/cellulose (%)	7.3	7.1	7.2	7.2	7.1
Intrinsic viscosity (mL/g)	527	554	532	529	494
NFC suspensions properties					
WRV (g H_2O/g NFC)	17.2	13.4	11.3	7.6	5.8
ÅA-GWR dewatering amount (g/m^2)	375	498	523	571	672
Average fibril thickness (nm)	6.5 ± 1.9	8.7 ± 2.3	11.7 ± 2.9	12.8 ± 3.0	16.1 ± 4.8
Average lignin particle size (nm)	–	26.6 ± 3.5	37.3 ± 8.7	42.8 ± 11.8	86.0 ± 23.3
Surface charge (μmol/g)	21.5	20.2	19.4	17.1	14.6
NFC films properties					
Lignin surface coverage (%)	2.2	4.2	6.2	7.5	10.3
Tensile strength (MPa)	92.16	97.11	83.44	81.99	90.78
Young modulus (GPa)	8.22	8.92	8.18	7.68	8.10
Breaking strain (%)	1.43	1.39	1.23	1.33	1.44
Water contact angle (5 s)	26.30	34.98	40.79	41.97	42.29

%odp percent on oven-dried pulp

fibrillar agglomerates in the matrix, the data variation of the rheometrical measurements was within ± 10%. This is considered acceptable considering the sample complexity including structuration and gelation. Rheological data contained mechanical noise, therefore they were smoothened by the Tikhonov regularization.

Results and discussion

Characterization of pulps, NFC suspensions and NFC films

The chemical composition of the pulps from which the NFC suspensions were produced are summarized in Table 1. In the lignin-containing pulps, the amount of lignin covalently bound to the fibers was 1.7%, corresponding to the lignin content of the low-lignin (L–L) pulp (Table 1). This was the amount of lignin that remained within the fibers even after extensive washing with an ethanol solution of 60 wt% concentration, which has been proven an efficient solvent for lignin dissolution (Ni and Hu 1995). In the other lignin-containing pulps, the higher lignin contents originated from the incomplete washing of the fibers and the subsequent re-absorbance of lignin onto the fiber surface upon water addition during washing.

Xylan, the main hemicellulose in *Eucalyptus* wood, is a water binding polysaccharide, and its presence on the nanocellulose fibrils has been shown to have a significant influence on the gelation and rheology of NFC (Pääkkönen et al. 2016). Moreover, the degree of polymerization (DP) of cellulose also has an influence the rheological properties of NFC suspensions (Shinoda et al. 2012; Strlič et al. 1998). In this work, the four lignin-containing pulps were produced from the same GVL/water fractionation experiment, with the only difference being the intensity of the lignin washing process. The hemicellulose/cellulose ratio and the cellulose DP in all the lignin-containing pulps was comparable (Table 1) and thus their influence on the rheological properties of NFC could be excluded. The small differences in pulp viscosity observed in Table 1 were likely caused by the different lignin content in the pulps. The fractionation and bleaching conditions to produce the fully bleached reference pulp (No–L) were chosen in such a way that the viscosity and hemicellulose/cellulose ratio of the pulp would be comparable to those of the lignin-containing pulps. Therefore, differences in the rheological behavior of the pulps could be solely attributed to the varying lignin content.

Fig. 2 **a** AFM height images (2 × 2 μm^2) and **b** SEM images (30 k magnification) of 5 NFC samples with varying residual lignin content. **c** SEM images (30 k magnification) showing the morphology of individual fibers of 2 NFC samples with the lowest and highest residual lignin content. The green arrows point to some lignin nanoparticles. (Color figure online)

The surface chemical composition of the self-supporting NFC films was evaluated with XPS after acetone extraction, as presented in Table 1. The XPS spectra are shown in Appendix B. Apart from the No–L NFC sample, the surface lignin contents of the four lignin-containing films were similar to the bulk lignin contents, suggesting that the residual lignin was well dispersed within the fibrillary film matrix. This is interesting, as in the case of natural fibers, the surface region is typically enriched with lignin (Koljonen et al. 2003). In the case of the No–L NFC film, the increase in the non-cellulosic C–C peaks most probably originates from the enhanced surface activity of the neat nanocellulose when exposed to the very dry measurement environment (ca. 10^{-9} Torr). Solvent exchange via acetone extraction stabilized these cellulosic surfaces (Johansson et al. 2011), however we could observe a marked increase in the non-cellulosic carbon in the XPS data for the non-extracted No–L NFC sample (data not shown), as well as the variations from sample to sample in the unextracted films with lignin additions. This is a typical phenomenon with extracted nanocellulosic samples measured without solvent exchange (Johansson et al. 2011).

The limited lignin-enrichment on the NFC films, as confirmed by XPS analysis, was also reflected on the slow increase of water contact angle with increasing lignin content. However, lignin-enrichment was previously achieved on NFC film produced by the same technique from residual lignin-containing pulp produce by SO_2–Ethanol–Water pulping of Norway spruce (Rojo et al. 2015), resulting in a water contact angle of 78° for the sample with highest lignin content of about 14%. Rojo et al. reported the softening of softwood lignin during hot pressing due to the suppression of its glass transition temperature from 135 to 80–90 °C by the plasticizing effect of water

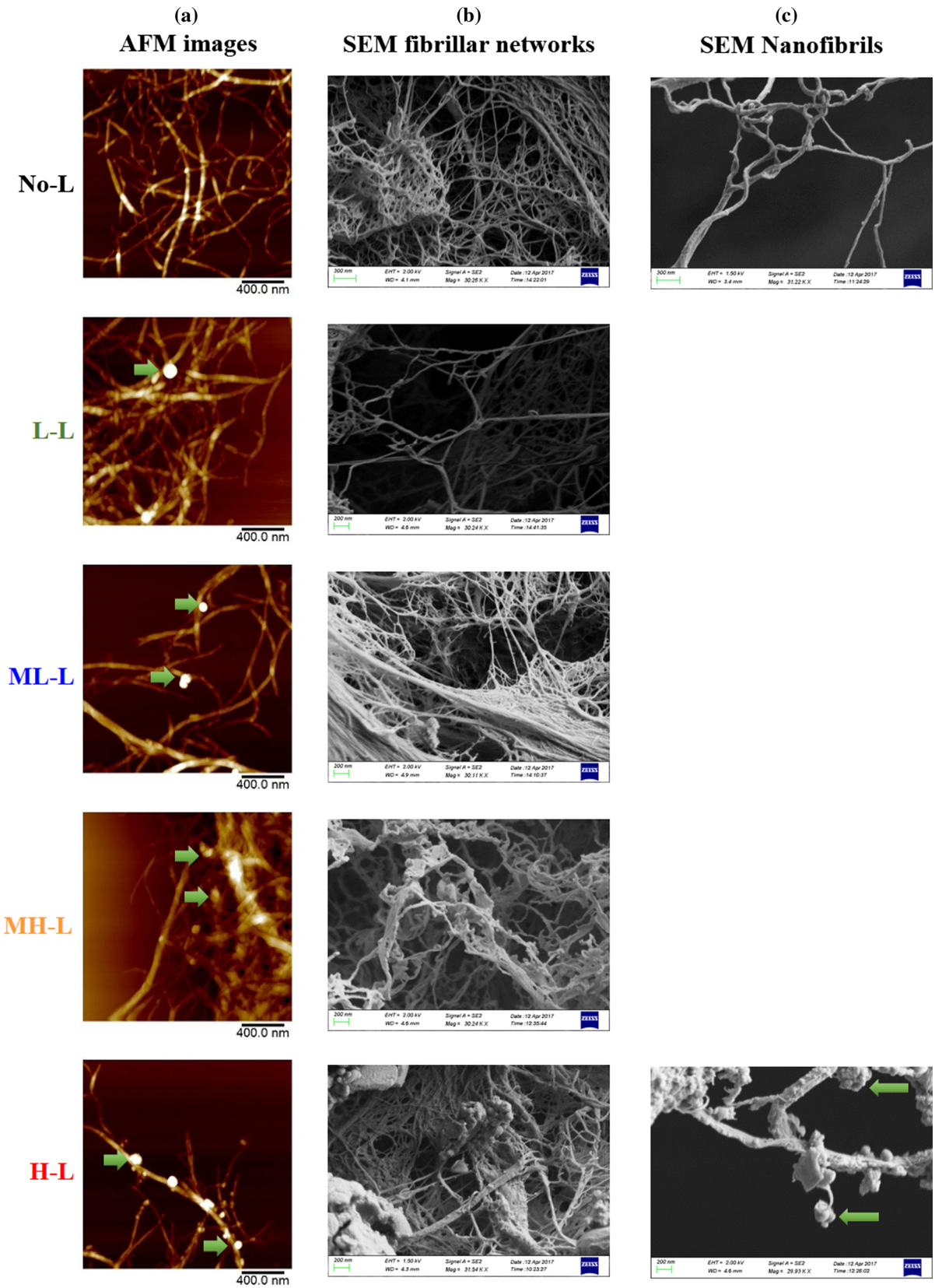
(a)
AFM images
(b)
SEM fibrillar networks
(c)
SEM Nanofibrils
No-L
L-L
ML-L
MH-L
H-L
400.0 nm
400.0 nm
400.0 nm
400.0 nm
400.0 nm

presented in the system (Rojo et al. 2015). In our case, eucalyptus GVL lignin has higher glass transition temperature of about 143 °C (Appendix C). Moreover, without the hydrophilic sulfonate group (introduced in SEW fractionation), GVL lignin probably exhibits lower affinity to water, resulting in a less pronounce plasticizing effect. Therefore, at the hot-pressing temperature of 100 °C, lignin particles in our samples might not be properly melted and spread over the surface of the NFC films, resulting in a similar lignin content on the surface to the bulk phase, which explain the limited increase in water contact angle as well as the slightly reduced mechanical properties of the films with increasing lignin content as reported in Table 1.

It can be concluded that the current conditions of the NFC films preparation method employed in this work are not compatible with our NFC material. In order to enhance the hydrophobicity of the film surface by lignin-enrichment, either the temperature during hot-pressing must be increased or another film preparation technique should be considered.

Topography and morphology of NFC

The fibrillar structure of NFC-gels produced from GVL/water pulps with varying lignin content were observed with AFM. The AFM images (Fig. 2), were recorded from the dried NFC-gel samples without any fractionation methods applied for maintaining the actual fibrillar structure. The AFM images indicate that all the pulps were effectively fibrillated into nanofibrillar scale excluding observable large fibril flocks generated upon drying of the NFC suspensions on the support. The AFM technique gives accurate values only to the Z-direction due to the image artifacts related to the size of AFM probehead (Orelma et al. 2012; Pääkkö et al. 2007). The removal of lignin by pulp washing from 10.5 to 1.7% resulted in the reduction of average fibril thickness from 16.1 to 8.7 nm (Table 1). The smallest fibril was observable for fully bleached sample with average thickness of about 6.5 nm. Besides, the lignin nanoparticles systematically grew in size with increasing residual lignin content in the NFC suspensions, from 26.6 nm (L–L sample) to 86.0 nm (H–L sample).

AFM gave useful information on the dimensions of the NFC and lignin particles, however, the preparation method of dry-casting induced the collapse of the fibril network, thus rendering the morphology of the NFC less visible on AFM images. For example, AFM height images (Fig. 2) suggest an unclear trend in the increase of lignin nanoparticle population when residual lignin content increases. However, most of the lignin particles were trapped in the collapsed fibril matrix, leaving only a few particles visible on the edges of the investigated area. Hence, the representativeness of the trend is questionable. Therefore, SEM images of freeze-dried NFC aerogels was recorded for revealing the preserved structure and lignin-fibril distribution within the NFC network. At higher residual lignin content, the surface of the fibrils appeared to be rougher with the coarse, globular lignin particles (Fig. 2). This confirms the vague trend hinted by the AFM images.

Rheology and dewatering of NFC suspensions

As the viscoelastic response of the NFC suspension structures depends on the morphology and the surface charge of the fibrils, uneven distribution of residual lignin on the fibril surface and within the suspension matrix has an influence on the swelling and rigidity of the NFC suspensions. The results from oscillatory measurements (Fig. 3a, b) distinguished the microstructure of NFC suspensions within the LVR by tracing the behavior of elastic moduli (G') and loss moduli (G'') from amplitude sweep measurements. As presented in Fig. 3a, the span of critical strain (γ_c), which defined the LVR and was presented with the decrease of moduli at higher strains amplitude, was higher for suspensions with lower residual lignin content. That phenomenon revealed the difference between the agglomeration and flocculation within the fibrillar matrix due to the varying surface charge of the fibrils and the glue-like effect of the residual lignin particles which were present both on the fibril surface and between the fibrils. Similar observation regarding the flocculation within the suspension as a response to varying residual lignin content and its effect on elasticity within the suspension can be seen through the moduli respond to increasing angular frequency (Fig. 3b). With increasing angular frequency (ω), agglomerated fibrils exhibited different rearrangement times. G' and G'' increased more rapidly for lignin-containing NFC suspensions (ML–L, MH–L and H–L), which also showed higher magnitudes of G' and G'' at lower angular frequency (ω). The absence of lignin increased the fibril surface charge (Table 1) and the

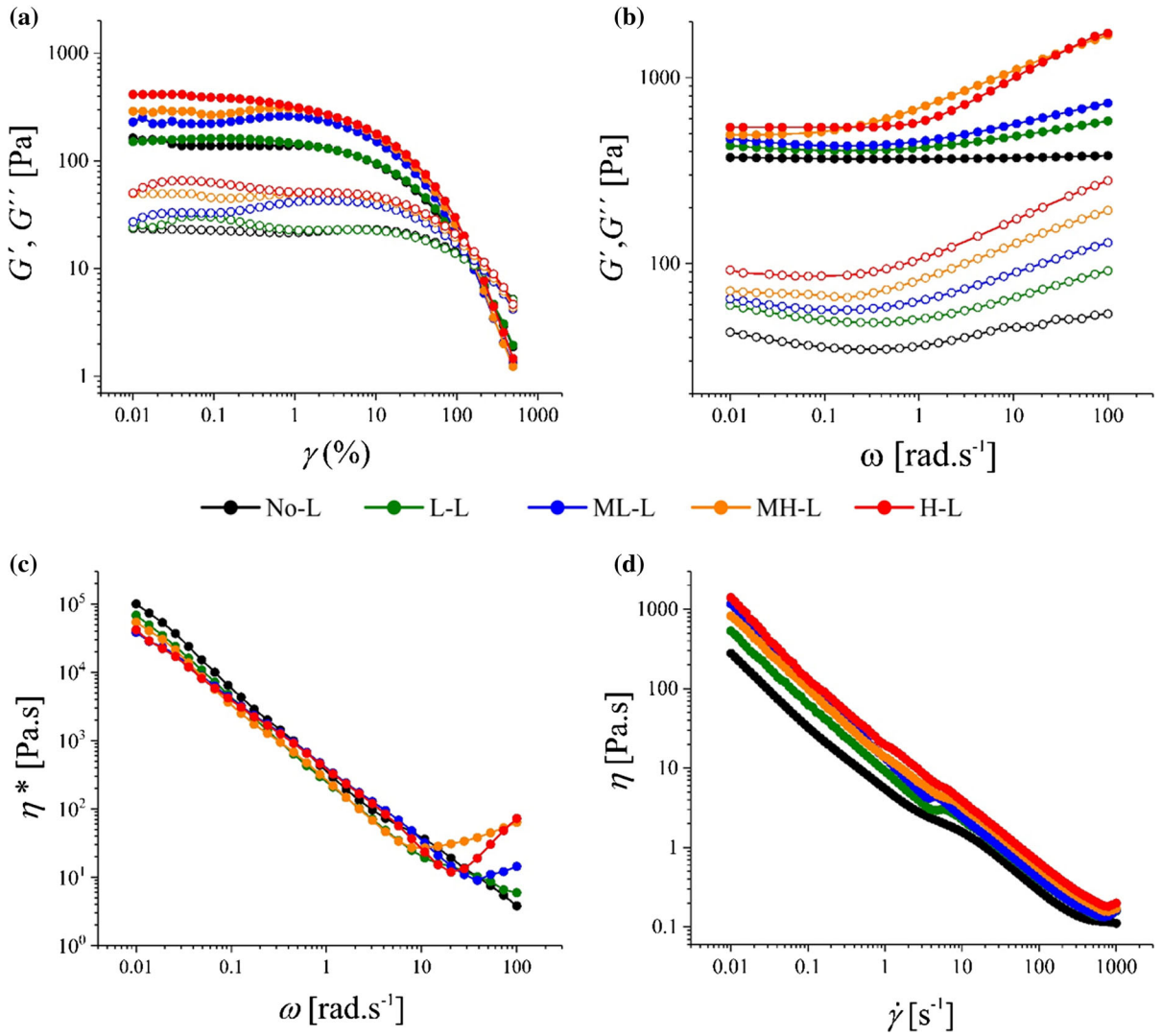

Fig. 3 Results from viscoelastic measurements of NFC suspensions at 1% consistency. Storage modulus (G′) and loss modulus (G″) are illustrated by closed and open symbols, respectively. **a** G′ and G″ as a function of strain ($\gamma = 0.01$–500%) at constant angular frequency $\omega = 1$ rad s^{-1} in amplitude sweep measurements. **b** G′ and G″ as a function of increasing angular frequency ($\omega = 0.1$–100 rad s^{-1}) in frequency sweep measurement **c** Complex viscosity (η*) as a function of angular frequency (ω). **d** Dynamic viscosity (η) as a function of increasing shear rate. (Color figure online)

gelation within network matrix, which was expressed as the independence of G′ and G″ from the angular frequency (ω). Therefore, the difference in moduli response to angular frequency (ω) reflected the difference between the swollen fibrils with higher surface charge (No–L and L–L samples) and the coarser, more flocculated one (MH–L and H–L samples). Also both Fig. 3a, b illustrate a distinguished grouping between NFC suspensions in terms of varying residual lignin content as lignin-rich group I (ML–L, MH–L and H–L samples) and lignin-lean group II (L–L and No–L samples). The values of G′ and G″ for the wide span of angular frequency are twice to five times higher for group I samples in comparison to those of group II.

Different levels of aggregation within the NFC suspensions were expressed as the response of the complex viscosity (η*) to the increase of angular frequency (ω) (Fig. 3c) and of the dynamic viscosity (η) to the increase of shear rate ($\dot{\gamma}$) (Fig. 3d). Figure 3c

presents the decrease of complex viscosity (η*) as a response of increasing deformation via angular frequency-dependent shear thinning, that reveals the shear thinning behavior for all suspensions with dilatant behavior at higher angular frequency for the samples of group I. The flow curves of dynamic viscosity (η) presented in Fig. 3d reveals a strong shear thinning behavior and the dilatancy at higher deformation for all the samples. The increase of both complex and dynamic viscosity at higher deformation can be explained with the deformation-induced aggregation of the lower surface-charged and more flocculated group I NFC suspensions containing lignin particles with glue-like properties (Fig. 2), which reduces the freedom of movement.

Complex viscosity (η*) reveals that the NFC suspensions exhibited distinct shear thinning behavior, with η* being dependent on the flocculation, and/or agglomeration, within the NFC matrix and the presence of residual lignin particles within it. The removal of lignin prior to fluidization influenced the surface charge of NFC fibrils, which in turn had an effect on the amount of water bound to the fibril surface and the gelation within the suspension. The values of η* as a function of shear rate follow a power law index (n), Eq. 1. Similarly, greater flocculation tendency of lignin-rich NFC suspensions was demonstrated by higher flow index k(η*), as shown in Table 2.

As demonstrated in Fig. 4a, b, similarly, the static yield stress τ_s^0, obtained from the amplitude sweep measurement within the linear viscoelastic region (LVR) was higher than the dynamic yield stress τ_d^0, measured when the suspension matrix was broken due to shearing.

Table 2 Rheological properties of the NFC suspensions

	No–L	L–L	ML–L	MH–L	H–L
$G'_{0.17\ \mathrm{rad\,s^{-1}}}$ [Pa]	278.1	299.5	317.1	344.6	415.1
$(G'/G'')_{0.5\%}$	3.78	3.21	2.82	2.75	2.12
$(G'/G'')_{1\ \mathrm{rad\,s^{-1}}}$	2.82	2.65	2.37	2.21	1.87
$\eta_{0.1\ \mathrm{s^{-1}}}$ (Pa.s)	45.1	61.8	98.2	110.1	144.2
$k(\eta^*)$	385.4	426.4	457.0	463.1	477.4
$n(\eta^*)$	0.03	0.04	0.09	0.17	0.22
$k(\eta)$	8.7	11.8	17.1	17.4	24.1
$n(\eta)$	0.19	0.21	0.32	0.33	0.35
τ_s^0 (Pa)	15.3	19.2	22.6	27.2	32.2
τ_d^0 (Pa)	8.1	13.1	14.4	15.4	18.5

Varying amount of residual lignin present on the fibril surface and within the suspensions affected both the flexibility and the surface charge of fibrils, resulting in the difference in the flocculation and the water binding gelation between group I and group II suspensions. This reflects the higher flocculation tendency of the thicker, lignin-rich NFC fibrils comprising a lower surface charge (group I), in comparison with the thinner ones comprising a higher surface charge (group II). An increase of lignin content resulted in a higher extent of flocculation of group I samples due to the diminution of fibril surface charge, which induced an increase of static yield stress (τ_s^0) in respect to the work required to break the fibrils agglomerates. The methods by which yield stress is measured (geometry) and calculated (curve fitting) significantly influence the results. As previously reported (Pääkkönen et al. 2016), there is a difference in the magnitude of yield stress values obtained within the LVR region (by oscillatory measurements) and in the shearing regime, when the viscoelastic structure of the suspension was broken and the fibrils aligned. Our samples exhibit a higher static yield stress (τ_s^0) in comparison to the dynamic yield stress (τ_d^0) (Table 2), which is a typical rheological feature of fibrillar gel-like NFC suspensions (Dimic-Misic et al. 2013b).

Due to the high dependence of the moduli (G′ and G″) on angular frequency for lignin-containing NFC suspensions (Fig. 3b) their values are presented at low values of 0.17 rad s^{-1} (Table 2). The lower surface charge and higher flocculation tendency of the lignin-containing samples raised the viscosity and moduli of the suspension (Dimic-Misic et al. 2013a), resulting in a stiffer gel. This was illustrated by the G′/G″ ratio at low strain ($\gamma = 0.5\%$) and at low angular frequency ($\omega = 1$ rad s^{-1}) (Table 2), which revealed the difference in gelation properties of the NFC suspensions and the increase in flocculation for the thicker and lower surface charged lignin-containing NFC fibrils. The higher mobility of the thinner fibrils of group II suspensions is expressed through lower values of the flow indices k(η) and k(η*) and through higher values from power law coefficient n(η), and n(η*) obtained from Eq. (1), as shown in Table 2.

Friction and agglomeration between fibrils increased with an increasing amount of residual lignin due to the coarser and thicker lower-charged fibrils

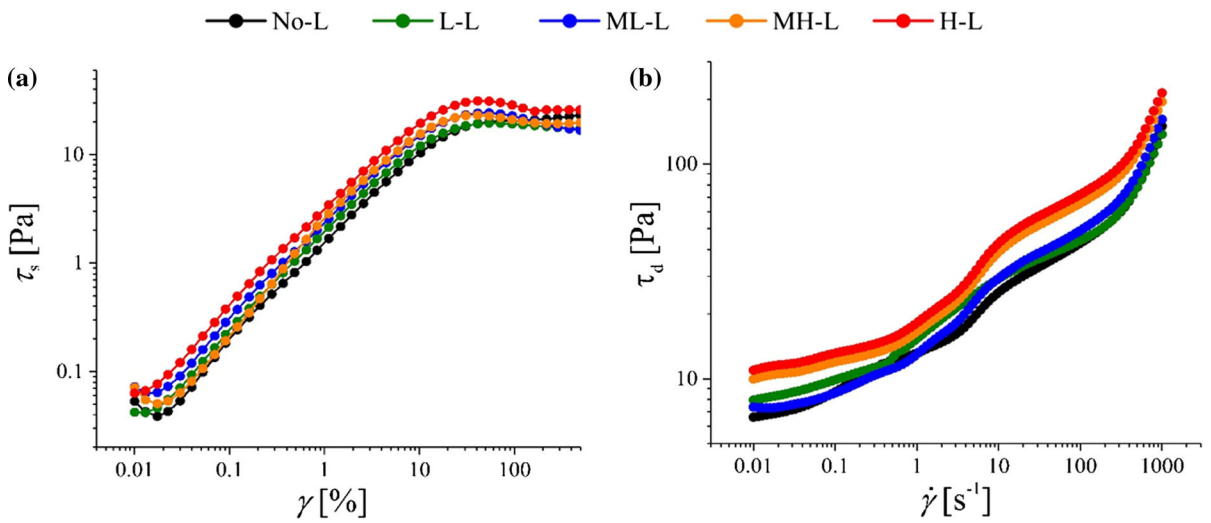

Fig. 4 **a** Static stress response to increasing strain amplitude and static yield stress (τ_s^0), as obtained from amplitude sweep measurements and Eq. 3. **b** Dynamic stress response to increasing shear rate and dynamic yield stress (τ_d^0), as obtained from Eq. 2. (Color figure online)

which were glued by the hydrophobic lignin particles present in the suspension matrix (Fig. 2). This phenomenon limited the gel-formation and water-holding capacity of the lignin-rich suspensions (group I), resulting in a more efficient dewatering, as reported for the ÅA-GWR experiments (Table 1).

Besides, better dewatering makes lignin-containing NFC attractive for application involving surface modification and composite synthesis. These applications are usually conducted in organic media, which require the complete removal of water before the reaction or composite suspension blending. A lower water retention would ease the effort on solvent exchange, thus improving the economic feasibility of the process.

Figure 5 presents the time dependent structure regeneration after the removal of high shear rate, which is reflected in the transient viscosity (η^+) and elasticity (G') 3ITT recovery experiments. After the breakdown of elastic gel-like structure at high shear during the second interval, the recovery to the pre-shear state (η_0 and G'_0, respectively) was highly dependent on the amount of residual lignin and, correspondingly, the aggregation within the NFC suspensions. In the viscosity recovery test, when low shear rate was reapplied at the beginning of the third interval, there is a competition between build-up forces related to the thixotropic behavior of the suspensions, and the shear flow forces tending to disrupt the on-going build up structure, resulting in an oscillatory behavior of the recovery curve. This phenomenon is more pronounced for samples from group I. In the elasticity recovery test, for highly flocculated samples (group I), the recovery after high shear exhibit a distinguishable overshoots due to the spring-like effect caused by the re-establishment of the flocculated aggregates (Pääkkönen et al. 2016), facilitated by the presence of hydrophobic lignin particles suspended between fibril aggregates, which acted as a glue. Similar rheological response of elastic structure of samples from group I was presented as the "elasticity hardening", i.e. the sudden increase of the elastic moduli (G', G'') magnitude at high angular frequencies (ω). The absence of the overshoot and more uniform structure recovery (for both elasticity and viscosity) was evident for the lignin-lean samples from group II, which was characterized by the higher mobility of fibrils. 3ITT recovery experiment is consistent with the dewatering tendency of the NFC suspensions as higher elasticity and elasticity recovery of suspensions induced by flocculated fibrils aggregates indicates improved phase separation properties with increasing residual lignin content.

The behavior of lignin containing NFC suspensions in 3ITT viscosity recovery tests can be implemented to, for example, surface coating application. Leveling and sagging are two important parameters to be controlled during coating on a substrate. Proper leveling requires lower viscosity and elasticity while high sagging results from too low viscosity recovery after the application of high shear (Dimic-Misic et al.

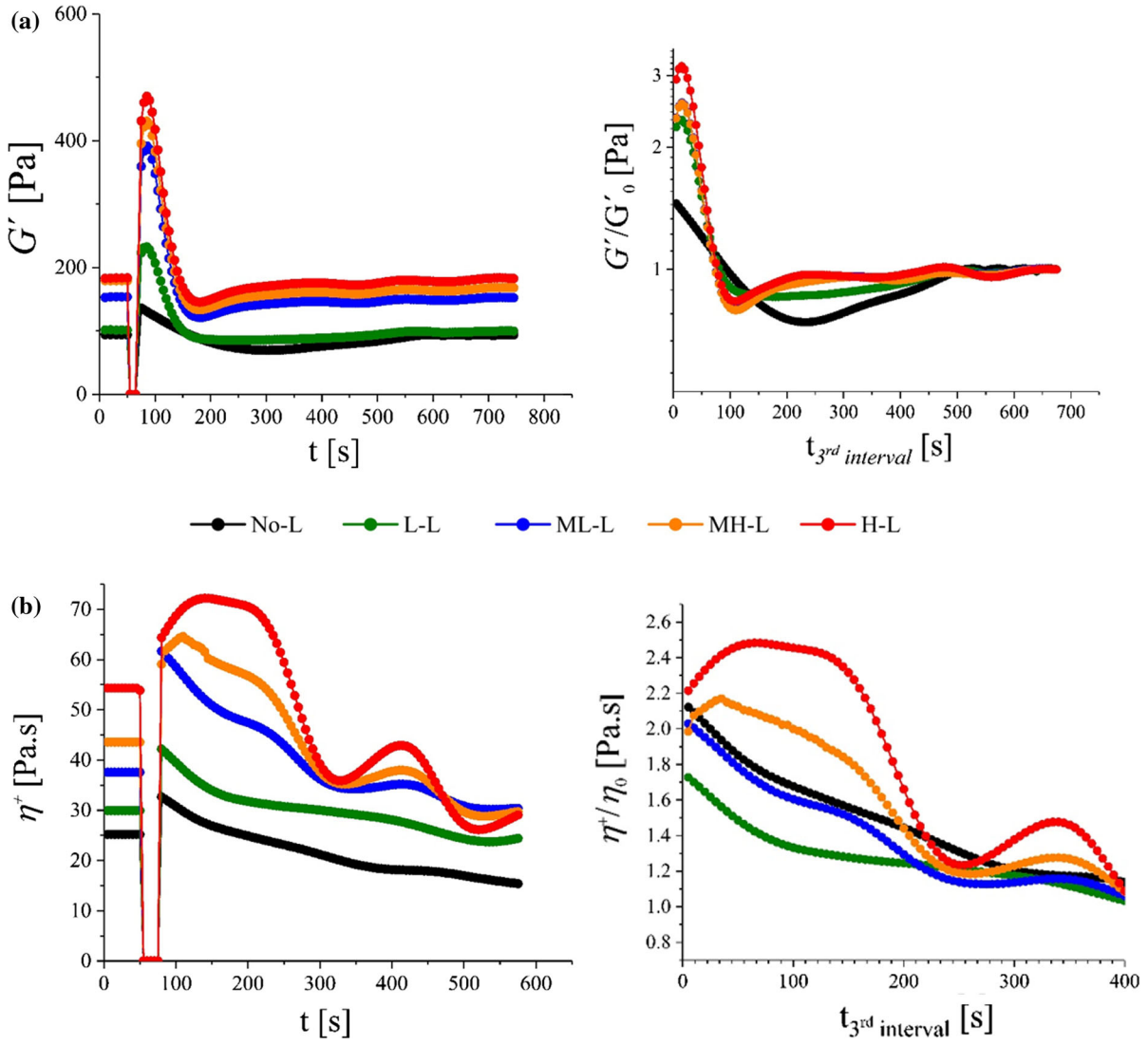

Fig. 5 Structural recovery in 3ITT experiments plotted as: **a** Elasticity recovery (G′) in oscillatory test with normalized elasticity (G′/G′$_0$). **b** Transient viscosity recovery in rotational test with normalized transient viscosity (η^+/η_0). (Color figure online)

2014c). Knowledge on the viscosity recovery is the basis of the selection of a proper coating protocol employing lignin containing NFC.

Conclusions

The presence of hydrophobic lignin remaining on the fibril surface and co-existing as particles within the suspensions matrix significantly influenced the morphology of fibrils and the corresponding flocculation and agglomeration tendency within the nanocellulose gel-like matrix. Moreover, the residual lignin which was removed from the fibrils but remains within the suspension significantly increased the flocculation and aggregation of the NFC. The presence of lignin also influences the level of aggregation and elasticity within the nanocellulose gel-network, improves the water-releasing properties, and increases the structure elasticity. The rheological properties of NFC suspensions containing residual lignin may be employed towards applications such as coating, surface modification and composite formation.

Acknowledgments Funding from Aalto University, School of Chemical Technology and Finnish Bioeconomy Cluster Oy (FIBIC) via the Advanced Cellulose to Novel Products (ACel) research program is gratefully acknowledged. This work made use of Aalto University Bioeconomy Facilities. The authors would like to thank Ms. Ritva Kivelä for her support with the NFC suspensions production, Dr. Kaarlo Nieminen for his support with the mathematical solutions, Ms. Rita Hataka for her support with the chromatographic analyses, Dr. Juan José Valle-Delgado for his advices on AFM image analysis, Dr. Krista Vajanto for her support on SEM images acquisition, Dr. Michael Hummel, Dr. Marc Borrega and Prof. Eero Kontturi for their advices on the manuscript.

References

Bonn D, Coussot P, Huynh HT, Bertrand F, Debrégeas G (2002) Rheology of soft glassy materials. Europhys Lett 59:786–792

Buscall R (2010) Letter to the editor: wall slip in dispersion rheometry. J Rheol 54:1177–1183. https://doi.org/10.1122/1.3495981

Chaari F, Racineux G, Poitou A, Chaouche M (2003) Rheological behavior of sewage sludge and strain-induced dewatering. Rheol Acta 42:273–279. https://doi.org/10.1007/s00397-002-0276-5

Conley K (2014) Annual review of global pulp and paper statistics. RISI Inc, PPI

Dalpke B, Kerekes RJ (2005) The influence of fibre properties on the apparent yield stress of flocculated pulp suspensions. J Pulp Paper Sci 31:39–43

Dentel SK, Abu-Orf MM, Walker CA (2000) Optimization of slurry flocculation and dewatering based on electrokinetic and rheological phenomena. Chem Eng J 80:65–72. https://doi.org/10.1016/S1383-5866(00)00078-2

Dimic-Misic K, Puisto A, Gane P, Nieminen K, Alava M, Paltakari J, Maloney T (2013a) The role of MFC/NFC swelling in the rheological behavior and dewatering of high consistency furnishes. Cellulose 20:2847–2861. https://doi.org/10.1007/s10570-013-0076-3

Dimic-Misic K, Puisto A, Paltakari J, Alava M, Maloney T (2013b) The influence of shear on the dewatering of high consistency nanofibrillated cellulose furnishes. Cellulose 20:1853–1864. https://doi.org/10.1007/s10570-013-9964-9

Dimic-Misic K, Nieminen K, Gane P, Maloney T, Sixta H, Paltakari J (2014a) Deriving a process viscosity for complex particulate nanofibrillar cellulose gel-containing suspensions. Appl Rheol 24:35616–35625. https://doi.org/10.3933/ApplRheol-24-35616

Dimic-Misic K, Nieminen K, Sixta H, Paltakari J, Maloney T (2014b) Processing plate immobolization data of nanocellulose furnishes. J Appl Eng Sci 12:145–152. https://doi.org/10.5937/jaes12-5021

Dimic-Misic K, Salo T, Paltakari J, Paltakari J (2014c) Comparing the rheological properties of novel nanofibrillar cellulose-formulated pigment coating colours with those using traditional thickener. Nord Pulp Pap Res J 29:253–270

Fall A, Bertrand F, Ovarlez G, Bonn D (2009) Yield stress and shear banding in granular suspensions. Phys Rev Lett 103:178301

Ferrer A, Quintana E, Filpponen I, Solala I, Vidal T, Rodriguez A, Laine J, Rojas OJ (2012) Effect of residual lignin and heteropolysaccharides in nanofibrillar cellulose and nanopaper from wood fibers. Cellulose 19:2179–2193. https://doi.org/10.1007/s10570-012-9788-z

Fukuzumi H, Saito T, Iwata T, Kumamoto Y, Isogai A (2009) Transparent and high gas barrier films of cellulose nanofibers prepared by TEMPO-mediated oxidation. Biomacromolecules 10:162–165. https://doi.org/10.1021/bm801065u

Huber GW, Iborra S, Corma A (2006) Synthesis of transportation fuels from biomass: chemistry, catalysts, and engineering. Chem Rev 106:4044–4098. https://doi.org/10.1021/cr068360d

Janardhnan S, Sain MM (2007) Isolation of cellulose microfibrils—an enzymatic approach. BioResources 1:176–188

Janson J (1970) Calculation of the polysaccharide composition of wood and pulp. Pap Puu 52:323–329

Johansson L, Campbell JM (2004) Reproducible XPS on biopolymers: cellulose studies. Surf Interface Anal 36:1018–1022

Johansson L, Tammelin T, Campbell JM, Setala H, Osterberg M (2011) Experimental evidence on medium driven cellulose surface adaptation demonstrated using nanofibrillated cellulose. Soft Matter 7:10917–10924. https://doi.org/10.1039/C1SM06073B

Karppinen A, Saarinen T, Salmela J, Laukkanen A, Nuopponen M, Seppälä J (2012) Flocculation of microfibrillated cellulose in shear flow. Cellulose 19:1807–1819. https://doi.org/10.1007/s10570-012-9766-5

Klemm D, Heublein B, Fink H, Bohn A (2005) Cellulose: fascinating biopolymer and sustainable raw material. Angew Chem Int Ed 44:3358–3393. https://doi.org/10.1002/anie.200460587

Koljonen K, Österberg M, Johansson L-, Stenius P (2003) Surface chemistry and morphology of different mechanical pulps determined by ESCA and AFM. Colloids Surf Physicochem Eng Asp 228:143–158. https://doi.org/10.1016/S0927-7757(03)00305-4

Lasseuguette E, Roux D, Nishiyama Y (2008) Rheological properties of microfibrillar suspension of TEMPO-oxidized pulp. Cellulose 15:425–433. https://doi.org/10.1007/s10570-007-9184-2

Lê HQ, Ma Y, Borrega M, Sixta H (2016) Wood biorefinery based on gamma-valerolactone/water fractionation. Green Chem 18:5466–5476. https://doi.org/10.1039/C6GC01692H

Lieth H (1975) Primary Production of the Major Vegetation Units of the World. In: Lieth H, Whittaker RH (eds) Primary productivity of the biosphere. Springer, Berlin Heidelberg, pp 203–215

Martoia F, Perge C, Dumont PJJ, Orgeas L, Fardin MA, Manneville S, Belgacem MN (2015) Heterogeneous flow kinematics of cellulose nanofibril suspensions under shear. Soft Matter 11:4742–4755. https://doi.org/10.1039/C5SM00530B

Moan M, Aubry T, Bossard F (2003) Nonlinear behavior of very concentrated suspensions of plate-like kaolin particles in shear flow. J Rheol 47:1493–1504. https://doi.org/10.1122/1.1608952

Mohtaschemi M, Sorvari A, Puisto A, Nuopponen M, Seppälä J, Alava MJ (2014) The vane method and kinetic modeling: shear rheology of nanofibrillated cellulose suspensions. Cellulose 21:3913–3925. https://doi.org/10.1007/s10570-014-0409-x

Moon RJ, Martini A, Nairn J, Simonsen J, Youngblood J (2011) Cellulose nanomaterials review: structure, properties and nanocomposites. Chem Soc Rev 40:3941–3994. https://doi.org/10.1039/C0CS00108B

Nazari B, Kumar V, Bousfield DW, Toivakka M (2016) Rheology of cellulose nanofibers suspensions: boundary driven flow. J Rheol 60:1151–1159. https://doi.org/10.1122/1.4960336

Nechyporchuk O, Belgacem MN, Pignon F (2014) Rheological properties of micro-/nanofibrillated cellulose suspensions: wall-slip and shear banding phenomena. Carbohydr Polym 112:432–439. https://doi.org/10.1016/j.carbpol.2014.05.092

Nelson K, Retsina T, Iakovlev M, van Heiningen A, Deng Y, Shatkin JA, Mulyadi A (2016) American Process: Production of Low Cost Nanocellulose for Renewable, Advanced Materials Applications. In: Madsen LD, Svedberg EB (eds) Materials research for manufacturing: an industrial perspective of turning materials into new products. Springer International Publishing, Cham, pp 267–302

Ni Y, Hu Q (1995) Alcell® lignin solubility in ethanol-water mixtures. J Appl Polym Sci 57:1441–1446. https://doi.org/10.1002/app.1995.070571203

Orelma H, Filpponen I, Johansson L, Österberg M, Rojas OJ, Laine J (2012) Surface functionalized nanofibrillar cellulose (NFC) film as a platform for immunoassays and diagnostics. Biointerphases 7:61. https://doi.org/10.1007/s13758-012-0061-7

Österberg M, Vartiainen J, Lucenius J, Hippi U, Seppälä J, Serimaa R, Laine J (2013) A fast method to produce strong NFC films as a platform for barrier and functional materials. ACS Appl Mater Interfaces 5:4640–4647. https://doi.org/10.1021/am401046x

Pääkkö M, Ankerfors M, Kosonen H, Nykänen A, Ahola S, Österberg M, Ruokolainen J, Laine J, Larsson PT, Ikkala O, Lindström T (2007) Enzymatic hydrolysis combined with mechanical shearing and high-pressure homogenization for nanoscale cellulose fibrils and strong gels. Biomacromolecules 8:1934–1941. https://doi.org/10.1021/bm061215p

Pääkkönen T, Dimic-Misic K, Orelma H, Pönni R, Vuorinen T, Maloney T (2016) Effect of xylan in hardwood pulp on the reaction rate of TEMPO-mediated oxidation and the rheology of the final nanofibrillated cellulose gel. Cellulose 23:277–293. https://doi.org/10.1007/s10570-015-0824-7

Puisto A, Illa X, Mohtaschemi M, Alava MJ (2012) Modeling the viscosity and aggregation of suspensions of highly anisotropic nanoparticles. Eur Phys J E Soft Matter Biol Phys 35:6. https://doi.org/10.1140/epje/i2012-12006-1

Rojo E, Peresin MS, Sampson WW, Hoeger IC, Vartiainen J, Laine J, Rojas OJ (2015) Comprehensive elucidation of the effect of residual lignin on the physical, barrier, mechanical and surface properties of nanocellulose films. Green Chem 17:1853–1866. https://doi.org/10.1039/C4GC02398F

Rudraraju VS, Wyandt CM (2005) Rheological characterization of Microcrystalline Cellulose/Sodiumcarboxymethyl cellulose hydrogels using a controlled stress rheometer: part I. Int J Pharm 292:53–61. https://doi.org/10.1016/j.ijpharm.2004.10.011

Saito T, Isogai A (2004) TEMPO-mediated oxidation of native cellulose. The effect of oxidation conditions on chemical and crystal structures of the water-insoluble fractions. Biomacromolecules 5:1983–1989. https://doi.org/10.1021/bm0497769

Saito T, Nishiyama Y, Putaux J, Vignon M, Isogai A (2006) Homogeneous suspensions of individualized microfibrils from TEMPO-catalyzed oxidation of native cellulose. Biomacromolecules 7:1687–1691. https://doi.org/10.1021/bm060154s

Sakurada I, Nukushina Y, Ito T (1962) Experimental determination of the elastic modulus of crystalline regions in oriented polymers. J Polym Sci 57:651–660

Sandas SE, Salminen PJ, Eklund DE (1989) Measuring the water retention of coating colors. Tappi J 17:207–210

Shinoda R, Saito T, Okita Y, Isogai A (2012) Relationship between length and degree of polymerization of TEMPO-oxidized cellulose nanofibrils. Biomacromolecules 13:842–849. https://doi.org/10.1021/bm2017542

Sjöström E (1993) Wood chemistry: fundamentals and applications. Academic Press, San Diego

Strlič M, Kolar J, Žigon M, Pihlar B (1998) Evaluation of size-exclusion chromatography and viscometry for the determination of molecular masses of oxidised cellulose. J Chromatogr A 805:93–99. https://doi.org/10.1016/S0021-9673(98)00008-9

Tanaka R, Saito T, Ishii D, Isogai A (2014) Determination of nanocellulose fibril length by shear viscosity measurement. Cellulose 21:1581–1589. https://doi.org/10.1007/s10570-014-0196-4

Usov I, Nyström G, Adamcik J, Handschin S, Schütz C, Fall A, Bergström L, Mezzenga R (2015) Understanding nanocellulose chirality and structure-properties relationship at the single fibril level. Nat Commun 6:7564

Yang MC, Scriven LE, MAcosko CW (1986) Some rheological measurements on magnetic iron oxide suspensions in silicone oil. J Rheol 30:1015–1029. https://doi.org/10.1122/1.549892

Young R (2014) World dissolving pulp monitor. RISI Inc, PPI